Available online at www.sciencedirect.com
SCIENCE DIRECT
Journal of Molecular Catalysis A: Chemical 243 (2006) 264–277
JOURNAL OF MOLECULAR CATALYSIS A: CHEMICAL
www.elsevier.com/locate/molcata

Epoxidation of propylene on Zn-treated TS-1 catalyst

V. Arca [a,*], A. Boscolo Boscoletto [a], N. Fracasso [a], L. Meda [b], G. Ranghino [b]

[a] *Polimeri Europa, Centro Ricerche, Via della Chimica 5, 30175 Marghera, Venezia, Italy*
[b] *Polimeri Europa, Centro Ricerche, Istituto G. Donegani, Via Fauser 4, 28100 Novara, Italy*

Received 23 May 2005; received in revised form 7 August 2005; accepted 7 August 2005
Available online 3 October 2005

Abstract

Direct propylene epoxidation with H_2O_2 performed on zinc salts pre-treated TS-1 has disclosed the specific role of zinc in the framework, changing the Ti-active site properties towards the reaction. When zinc is present, the donor property of the reaction solvent to Ti-site increases and the Ti–OOH electrophilicity reduces, giving rise to a high propylene oxide selectivity well-evidenced by a lower experimental by-product formation. Quantum mechanical calculations show that, regardless of zinc presence, the bond distances of substituents at titanium appears too large to justify the formation of a well-defined Clerici-like cycle. On the contrary, a larger cycle in which the silanol is shared between alcoholic and hydroperoxide groups coordinated on Ti-site results much more reasonable. We suggest the propylene epoxidation can occur at Ti-site by a cyclic reaction scheme in which a hydroperoxide oxygen abstraction by propylene double bond is promoted by a concerted electronic rearrangement and protonic transfer involving silanol and alcoholic groups to form water and propylene oxide.

Keywords: Propylene oxide; Epoxidation; Titanium silicalite; Hydrogen peroxide; Zinc

1. Introduction

Titanium silicalite-1 (TS-1) shows a remarkable high efficiency and molecular selectivity in oxidation reactions employing H_2O_2 under mild conditions such as the conversions of ammonia to hydroxylamine, of secondary alcohols to ketones and of secondary amines to dialkylhydroxylamines or reactions such as the phenol hydroxylation, the olefin epoxidation, the ketone ammoximation and also sulfide and disulfide oxidation [1–5]. For these reasons TS-1 has become one of the most relevant oxidation industrial catalysts in the last 20 years. The aim of our work was to verify the TS-1 activity in the epoxidation reaction of propylene, when it is treated with a metal cation such as zinc, thought in the first place as a TS-1 acidity inhibitor, to reduce and control the propylene oxide solvolysis. On the other hand, the investigation has suggested a specific zinc role, as direct consequence of its coordination to Ti-site, inducing a peculiar variation in the property of the active centre towards the epoxidation reaction. Experimental data and quantum mechanical calculations performed during the study have so shown some important features, as far as concerning both the coordination of the metal ion within the TS-1 and some possible variations on the epoxidation mechanism till now accepted, also regardless of zinc presence.

2. Experimental

2.1. Materials and sample preparation

TS-1 catalyst, prepared following the original patent [6], has a titanium molar content of 0.023 (1.84 wt% TiO_2). XRD, DRS UV–vis and XPS analyses of TS-1 do not detect the presence of extra-framework titanium, in terms of its oxide, so that it can be considered all in isomorphous substitution to framework silicon. B.E.T. specific surface area, obtained by N_2 adsorption at the liquid nitrogen temperature, was 484 m^2/g.

Titanium silcalite was treated under reflux condition in water or in zinc acetate dihydrate aqueous solution, and then separated by decantation and filtration, rinsed under water reflux, dried and calcined as described in Table 1. The TS-1 catalysts were water-treated and calcined at 823 K (C1 sample) before zinc-treatment. Molarity of $Zn(OAc)_2{\cdot}2H_2O$ aqueous solution was 0.137 and the TS-1 suspension in the solution 30 g/l. Zinc content in the catalysts was measured by atomic absorption (AAS)

* Corresponding author. Tel.: +39 041 2913279; fax: +39 041 2912530.
E-mail address: vittorio.arca@polimerieuropa.com (V. Arca).

1381-1169/$ – see front matter © 2005 Elsevier B.V. All rights reserved.
doi:10.1016/j.molcata.2005.08.040

Table 1
TS-1 treatment under reflux condition in H_2O or $Zn(OAc)_2{\cdot}2H_2O$ aqueous solution; zinc content and aqueous slurry apparent pH

Sample	Agent	Calcinated for 5 h (K)	Zn (wt%)	Apparent pH
C0	H_2O	No	–	4.66
C1	H_2O	823	–	4.60
C2	H_2O	1073	–	4.63
C3	$Zn(OAc)_2{\cdot}2H_2O$	No	4.54	6.47
C4	$Zn(OAc)_2{\cdot}2H_2O$	823	4.28	6.70
C5	$Zn(OAc)_2{\cdot}2H_2O$	1073	4.50	6.20

C0, C1, C2: TS-1 samples treated with H_2O under reflux for 4 h then dried in vacuum.
C1, C2 : calcinated for 5 h at 823 and 1073 K, respectively.
C3, C4, C5 : C1 sample treated with zinc acetate under reflux for 4 h, H_2O rinsed, then dried in vacuum.
C4, C5 : calcinated for 5 h at 823 and 1073 K, respectively.

and reported in Table 1 together with the aqueous slurry apparent pH. The pH value was evaluated after each TS-1 treatments, dipping 5 g of catalyst in 1000 ml of Millipore water and keeping the slurry at 293 K under N_2 flow and 300 rpm constant stirring. The high zinc content in TS-1, obtained in these treatment conditions, has been thought in order to allow an accurate analytical characterization and visualize the Zn effect on TS-1 crystal.

2.2. Epoxidation reaction

2.2.1. Rapid evaluation test

In a 1-l reactor, equipped with a mechanical stirrer with gaseous effect and a thermostatic system (internal coil immersed in the reaction solution and external re-circulation jacket), 5 g of TS-1 catalyst (Zn treated and untreated) was suspended in 500 g of methanol. The system was thermostated at 313 K and pressurized with propylene at 2.2 atm, maintained constant for the whole duration of the test, under stirring. Then 16.23 g of hydrogen peroxide at 34.74 wt% were continually added per 15 min and, after this period, a sample of reaction solution was immediately collected on quenching at 243 K. The residue H_2O_2 was determined by iodometry whereas the reaction products were quantified by gas chromatography (GC-FID).

2.2.2. Kinetic test

In a 1-l reactor, equipped with a mechanical stirrer with gaseous effect (2000 rpm) and a thermostatic system (internal coil immersed in the reaction solution and external re-circulation jacket), a gas vent condenser and a sample capillary at 243 K, 2 g of TS-1 catalyst (Zn treated and untreated) was suspended in 460 g of methanol and 9.0 g of water. The system was thermostated at 313 K and propylene was added at 1 g/min rate, at the pressure of 2.2 atm, constant for the whole duration of the test. Then 30.77 g of hydrogen peroxide at 55.27 wt% were added in one shot. At regular time range two samples were collected by a needle valve joined to the capillary connection, dipped in a flask containing the dilution solvent, 40 ml of methanol and 0.3 g of propyl carbonate as internal standard, at 233 K, so avoiding samples evaporation. The residue H_2O_2 was determined by iodometry whereas the reaction products were quantified by GC-FID.

2.3. Characterization techniques

2.3.1. XPS analysis

XPS analyses were performed by a PHI-5500—Physical Electronics spectrometer, having a monochromatized source with aluminum anode (Kα = 1486.6 eV), at 400 W, 5.85 eV pass-energy, 0.05 eV energy-step and 10^{-9} Torr residue pressure. The spectrometer was calibrated assuming $Ag(3d_{5/2})$ binding energy (BE) at 368.3 eV with respect to the Fermi-level and the measured full width half maximum (FWHM) is 0.46 eV. In order to neutralize the surface electrostatic charge of the catalysts, being non-conductive, it was utilized an electron gun. Furthermore, the charging effect on the analysis was also corrected considering both the $Si(2p_{3/2})$ peak at 103.6 eV BE, characteristic of SiO_2, as internal reference [7] and the graphite peak at 285 eV due to intentional addition.

The BEs were measured from the maximum of the peaks, without any baseline subtraction, given their substantial symmetry. Plane surfaces were obtained by pressing the catalyst powders on an indium-base.

2.3.2. DRS UV–vis

UV–vis spectrophotometry was performed by Perkin-Elmer Lambda 9 in the wavelength range 200–400 nm at 1 nm/s scan rate. The instrument is equipped with integrating sphere, 60 mm Perkin-Elmer UV/vis/NIR, coated with barium sulfate film for diffuse reflectance spectroscopy (DRS) [8]. TS-1 catalyst was inserted into the quartz cell, dehydrated at 393 K for 5 h on dynamic vacuum and analyzed. The collected spectra were given in Kubelka–Munk unit.

2.3.3. XRPD

X-ray powder diffraction (XRPD) spectra were collected by Philips PW1050 diffractometer, having Bragg–Brentano geometry. PW1050 working conditions were: Cu Kα radiation nickel filtered, energy and current of 40 kV and 40 mA, 10–60°2Θ angular scan range at 0.02°2Θ step and 12.5 s each step, divergence (1/4°)–receiving (0.1 mm)–scattering (4°) slit configuration. The diffractometer was calibrated using silicon (Si, SRM 640c) and TiO_2 rutile standards. The Rietveld analysis of TS-1 spectra was performed using the GSAS program package, by Larson and Von Dreele [9,10]. In order to achieve a better accuracy by Rietveld refinement TiO_2 rutile was added as internal standard.

2.3.4. TGA

Thermogravimetric analyses (TGA) were performed by a Mettler-Toledo TGA/SDTA 851 thermobalance. TS-1 samples, about 30 mg, placed on Pt-pan were analyzed under 50 ml/min nitrogen flow on the following conditions: heated from 323 to 363 K at 20 K/min and kept at this temperature for 20 min, cooled at 323 K and reheated up to 1273 K at 5 K/min.

2.3.5. GC-FID

Gas chromatographic analysis for the determination of propylene oxide and by-products, glycols and ethers, resulting from epoxidation test was performed using Carlo Erba HRGC 5300 Mega Series with FID detector and Shimadzu C-R4A Chromatopack integrator. Wide bore Supelcowax 10 M column, having 60 m length, 0.53 mm i.d., 1.0 μm film thickness, was used for the separation on following conditions: 8 min at 333 K, then from 333 to 437 K at 6 K/min and 20 min at the higher. The gases were: nitrogen carrier at 5.7 ml/min, hydrogen at 30 ml/min, air at 300 ml/min. Retention times was determined using authentic samples of propylene oxide and products of its solvolysis 1-methoxy-2-propanol, 2-methoxy-1-propanol and 1,2-propanediol.

2.4. Molecular modelling

2.4.1. Quantum mechanical calculation

Ab initio quantum mechanical calculations employing density functional theory (DFT) were performed using Castep-Cerius^2 4.2 package, in which electronic wavefunctions are expanded through a plane-wave basis set with cutoff energy of 360 eV and local spin density approximation (LSDA), suitable to describe three-dimensional solids [11,12]. A cluster-like complex, isolated from the TS-1 crystal, having two adjacent rings with 10- and 5-tetrahedral units and inserted in a 15 Å cubic cell was used to investigate the interaction between $[Zn(OH)]^+$ cation and Ti-site (Section 3.6). Titanium atom in the complex is in T11 site [13], which is among the most accessible to the sorbate. As far as the complex optimization process is concerned, only silicon or titanium atom with their four-oxygen nearest neighbors, one $[Zn(OH)]^+$ cation and one water molecule were allowed to move. The optimization was achieved minimizing the energy gradient in function of second derivative of coordinates.

The interaction energy between methanol and TS-1 and the nuclear locations corresponding to local minima of the energy were calculated using FastStructure-Cerius^2 package, an ab initio code employing DFT method. Fast and accurate calculation is achieved by Harris functional [14]. The cluster model has the structure of the TS-1 crystalline cage with Ti atom in T11 site, composed by 14-tetrahedral units. The Ti–O–Si bond has been broken by H_2O_2 insertion with the formation of the Si–OH leaving group and of the hydroxonium anion (Ti–OOH group); zinc is in the framework forming a Zn–O–Ti bond. The geometry of the cage during the optimization was kept fix and only the Ti and Zn atoms, the three of four oxygen atoms covalently bound to the metals, the OOH group and the formed silanol are allowed to relax during the geometry optimization; the total charge was set equal to zero. The solvent/reactant molecules were free to move. The choice of these initial conditions for the model allows to obtain a conservative and favourable energetic situation, because the TS-1 crystal is considered and the highest freedom of mutual coordination of the substituents to Ti-site is obtained.

The basis set assignment was the *standard* orbital basis set in combination with the *enhanced* density basis set, as described in Cerius^2. Moreover, the core level was *all electron* for light atoms (hydrogen, oxygen, carbon) and *relaxed* for the heavy atoms (Si, Ti and Zn).

2.4.2. Statistical thermodynamics

The adsorption of sorbates like $[Zn(OH)]^+$ and H_2O into the S-1 and TS-1 crystal was performed using Sorption-Cerius^2 package that applies Monte Carlo statistical mechanics method and analytic interaction potential of van der Waals and Coulomb type, to simulate the loading and to evaluate the solvation energy. In the calculation the crystal is considered rigid, whereas sorbate molecules are free to rotate and translate into the pores and their number and position are updated and evaluated in each step. Adsorption energy and loading mean values are assumed to be stable after a number of configurations of the order of 10^6.

3. Results and discussion

3.1. TGA

C0 and C3 samples, respectively, treated in H_2O and in the zinc acetate aqueous solution (Table 1), were analyzed by TGA, after conditioning in the same thermobalance for a direct comparison (Fig. 1). Except for the first short part of curve related to the instrument transition from conditioning to measuring, two main variations for C0 are observed in weight loss range from 100 to 98.5 wt%: the first up to 353 K due to the loss of physisorbed water and the second up to 553 K to the displacement of coordinative and hydrogen bonded water. At higher temperature silanol and/or titanol condensation takes place, accompanied by structural rearrangements [15]. Similarly, the C3 curve shows a first variation at 373 K, followed by a weight loss up to 678 K due to leaving water and residual acetic acid. The subsequent weight loss up to 1273 K is lower then measured for C0 sample, as if a structure rearrangement

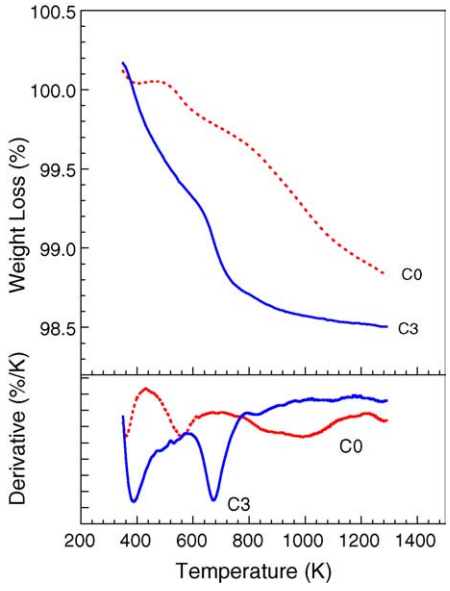

Fig. 1. TGA curves of C0, untreated TS-1 (dotted line), and C3, Zn-treated TS-1 (solid line); down, the first derivative.

(including hydroxyl condensation) was been anticipated for the zinc presence.

3.2. XRPD

TS-1 crystalline phase having orthorhombic symmetry is clearly observed by XRPD analysis of different samples, water-treated (C0–C2) and zinc-treated (C3–C5). Only C5, calcined at the higher temperature (1073 K), has got in addition a new phase identified as α-willemite (zinc orthosilicate, Zn_2SiO_4) with trigonal symmetry and *R*-3 space group [16]. The α-willemite lattice has two inequivalent Zn-sites, both having four nearest neighbor oxygen ions in slightly distorted tetrahedral configuration [17]. C2 (a) and C5 (b) spectra and their difference (c) are reported in Fig. 2. The thin bars in (c) show α-willemite phase (JCPDS 8-492 card). A painstaking analysis of C3–C5 spectra did not disclose ZnO, TiO_2 and possible $ZnTiO_3$ and Zn_2TiO_4 crystalline phases, clearly on the basis of the analytical detectability threshold. Rietveld refinement of XRPD spectra of treated TS-1 samples, to which TiO_2 rutile was added as internal standard, has displayed the effect of the different treatments on TS-1 cell parameters. The refinements were performed starting from TS-1 [13], TiO_2 rutile [18] and α-willemite [16] crystal data (lattice parameters, atomic coordinates and thermal parameters) and as example the calculated C5 spectrum is showed in Fig. 3. It was found that H_2O-treatment followed by calcination gives rise to cell volume contraction from 5368 $Å^3$ (823 K) to 5360 $Å^3$ (1073 K), whereas $Zn(OAc)_2$ treatment maintains an open structure with cell volume of 5370 $Å^3$ also after thermal annealing at 1073 K (Table 2). α-Zn_2SiO_4 refined parameters are reported in Table 3. It was calculated a willemite content of 9.30 (±1.75) wt%, in satisfactory concordance with the zinc amount measured via AAS. Also TiO_2 amount is resulted to be in good agreement with the added quantities. A silicalite-1 sample, S-1, having monoclinic symmetry was Zn-treated, in order to verify the titanium role in TS-1. The amount of Zn in S-1, treated at the C3 conditions, resulted quite limited (<0.3 wt%) if compared to C3–C5 samples (about 4.4 wt%) and willemite phase, after calcination at 1073 K,

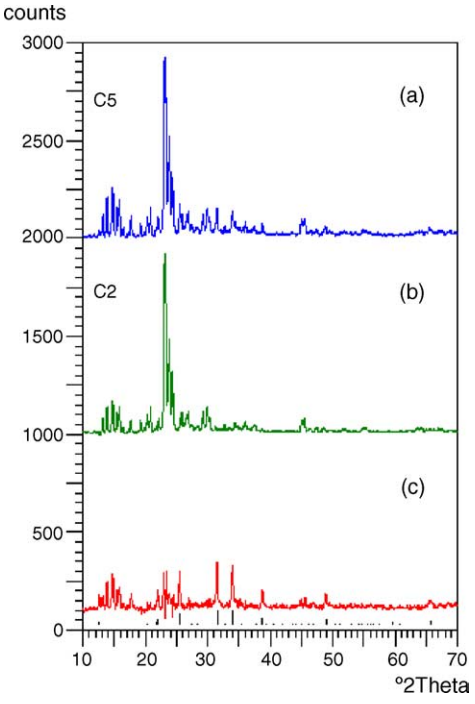

Fig. 2. XRPD spectra: (a) Zn-treated and (b) untreated TS-1, both calcined at 1073 K and (c) their difference; thin bars in (c) show the α-willemite phase.

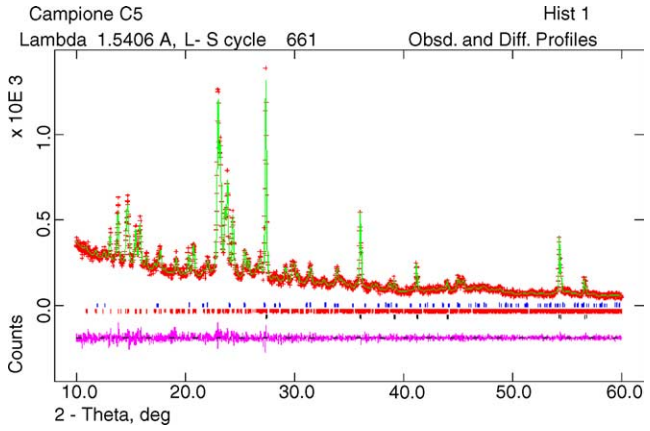

Fig. 3. Rietveld refinements: experimental (crosses) and calculated (solid upper line) powder diffraction spectrum of C5 sample and their difference (solid lower line).

Table 2
Rietveld refinement: TS-1 cell parameters

	H_2O[a]			$Zn(OAc)_2·2H_2O$[a]		
	C0[b] No[c]	C1[b] 823 K[c]	C2[b] 1073 K[c]	C3[b] No[c]	C4[b] 823 K[c]	C5[b] 1073 K[c]
a (Å)	20.1097(22)	20.1093(14)	20.0903(19)	20.1084(28)	20.1036(13)	20.1108(14)
b (Å)	19.9172(16)	19.9165(14)	19.9128(20)	19.9265(21)	19.9287(13)	19.9208(15)
c (Å)	13.4022(15)	13.4009(13)	13.3982(17)	13.4058(18)	13.4029(11)	13.4015(13)
Volume ($Å^3$)	5367.9(0.8)	5367.1(0.8)	5360.0(0.9)	5371.6(1.0)	5369.7(0.5)	5368.9(0.9)
χ^2	1.253	1.152	1.120	1.123	1.139	1.055
R_p	0.050	0.060	0.075	0.056	0.051	0.058
R_{wp}	0.065	0.079	0.103	0.073	0.066	0.075
D_{wd}	1.843	1.988	1.949	1.959	1.946	1.978

[a] Agent.
[b] Sample.
[c] Calcinated for 5 h.

Table 3
Willemite (α-Zn_2SiO_4) Rietveld refinement: cell parameters, atomic coordinates and thermal factors

Name	*X*	*Y*	*Z*	$U_i/U_e \times 100$	Site	Sym. mult	Type	Seq.	Fraction
Zn1	0.190(14)	0.206(15)	0.580(33)	69.3(4)	1	18	Zn	1	1.0000
Zn2	0.196(15)	0.218(91)	0.916(34)	72.7(4)	1	18	Zn	2	1.0000
Si3	0.196(20)	0.213(28)	0.244(10)	70.4(5)	1	18	Si	3	1.0000
O4	0.123(49)	0.202(51)	0.108(14)	93.9(3)	1	18	O	4	1.0000
O5	0.127(62)	0.203(32)	0.386(13)	73.6(3)	1	18	O	5	1.0000
O6	0.118(35)	0.226(43)	0.741(16)	83.2(1)	1	18	O	6	1.0000
O7	0.315(48)	0.329(48)	0.273(21)	96.2(8)	1	18	O	7	1.0000

Space group *R*-3. Lattice constants are: $a = 13.9555(31)$, $b = a$, $c = 9.3177(37)$; $\alpha = 90$, $\beta = 90$, $\gamma = 120$; cell volume = 1571.5(0.7).

was not detected. S-1 treatment in aqueous solution at double $Zn(OAc)_2$ molarity determined in the sample a significant presence of Zn (1.6 wt%). Therefore, for a correct comparison, a TS-1 sample was Zn-treated at the suitable solution molarity to have the same zinc content. At 823 K the two Zn-treated samples have shown only the respective TS-1 and S-1 phases, while at 1073 K willemite was observed in Zn/TS-1 sample, but not in Zn/S-1. From this finding, it is possible to affirm that the TS-1 zinc retention capacity is higher than S-1 one and that at the same zinc content the formation of α-willemite crystal phase, by calcination at 1073 K, is facilitated in TS-1 for the titanium presence which lowers the activation energy [19,20].

3.3. DRS UV–vis

Fig. 4 displays DRS UV–vis spectra, collected in the 200–400 nm range, of water-treated C0–C2 samples (a) and Zn-treated C3–C5 (b). The spectra in (a), at the increasing temperature, do not show among them any particular difference in terms of position (205 nm) and intensity of *LMCT* transition [21], pointing to that titanium is in tetrahedral coordination and isomorphous to Si(IV) in the silicalite framework. Moreover, after heating at 1073 K (C2) any absorption increase in the 250–350 nm range has not been observed that could indicate the formation of extra-framework TiO_2 nanoclusters via destructuration of isomorphous Ti(VI) [22]. The treatment with $Zn(OAc)_2$, C3 spectrum (b), gives rise to the shift of maximum from 205 to 211 nm accompanied by its intensity reduction and by absorption increase in the range 235–275 nm. The calcination at 823 K (C4) induces the reduction of this absorption, without restoring the original situation (C1), remaining almost unchanged the other parts of the spectrum. At 1073 K (C5) the absorption profile drastically changes showing a new maximum at 228 nm and a shoulder at 260 nm. The absorption then decreases down to 340 nm, but it remains in the 260–340 nm range, higher than the C3 and C4 spectra.

In addition to these samples, others were prepared to understand how zinc coordinates in the TS-1 framework. TS-1 samples were treated in $Zn(OAc)_2$ aqueous solutions at different molarities, so obtaining TS-1 at increasing Zn content. As previously observed, differences are not evident after calcination at 823 K, whereas at highest temperature (1073 K), as shown in Fig. 5, the *LMCT* maximum, as from 0.3 wt% zinc content, linearly shifts from 210 nm towards higher wavelengths (228 nm) and decreases in intensity. The absorption in the range 230–340 nm increases, showing then the shoulder at 262 nm.

On the strength of these first evidences, we propose that the maximum at 228 nm is related to an oxygen mediated interaction between Ti-site and Zn (Ti···O–Zn) or, as hypothesis, due to an Ti(IV) isomorphous substituted in α-Zn_2SiO_4. In addition to this, the absorption evolution at higher wavelength (from 250 nm up) could be related to TiO_2 and/or ZnO nanoparticles, even if XRPD does not detect them. In any case, the quantum mechanical calculation described by Brus [23–26] would give,

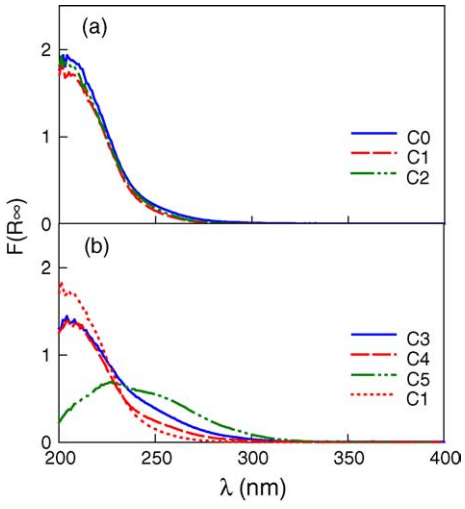

Fig. 4. DRS UV–vis spectra: (a) TS-1 and (b) Zn-treated TS-1 at increasing calcinations temperature.

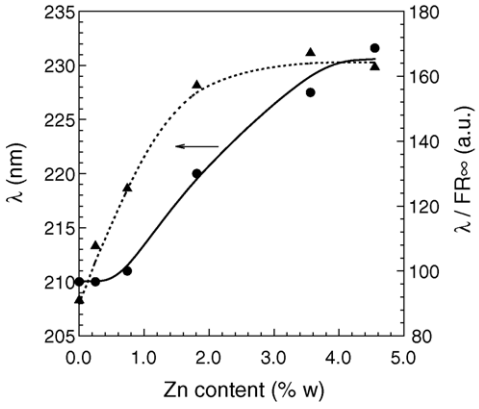

Fig. 5. DRS UV–vis λ_{max} vs. Zn-content in TS-1, calcined at 1073 K: (left ordinate) shift of λ_{max} and (right) λ_{max}/intensity ratio.

Table 4
XPS analysis: atomic concentration at the surface

	Agent	Calcinated for 5 h (K)	O(1s) (at.%)	Si(2p) (at.%)	Ti(2p) (at.%)	$Zn(2p_{3/2})$ (at.%)	C(1s) (at.%)
C0	H_2O	No	56.6	41.2	0.2	–	2.0
C1	H_2O	823	55.9	39.6	0.2	–	4.0
C2	H_2O	1073	58.0	39.0	0.2	–	2.8
C3	$Zn(OAc)_2{\cdot}2H_2O$	No	55.9	35.5	0.3	1.0	7.4
C4	$Zn(OAc)_2{\cdot}2H_2O$	823	53.2	35.9	0.4	0.9	8.7
C5	$Zn(OAc)_2{\cdot}2H_2O$	1073	55.4	38.1	0.5	0.9	5.1

taking as threshold the shoulder at 257 nm (4.8 eV), a cluster radius *R* of about 10 and 3 Å for ZnO and TiO_2, respectively.

3.4. XPS

High-resolution XPS was performed on C0–C5 samples, and on ZnO and $Zn(OAc)_2{\cdot}2H_2O$ standards, in order to analyze the TS-1 surface elemental composition in terms of BE and atomic concentration (at.%). The concentration values are reported in Table 4, showing for the two series, C0–C2 and C3–C5, a substantially similar Si and O content, within the standard deviation. The Zn-treated series C3–C5, with respect to C0–C2, shows a higher Ti and C content and the Zn presence. At the surface, Zn concentration is 0.9 at.% (about 2.8 wt%) and it results lower if compared with the 4.4 wt% of bulk zinc content, pointing out the cation easily diffuses into the TS-1 framework. The high carbon level is due to the organic introduced by the zinc acetate treatment that is additional to residual template and adventitious carbon.

The BE and the FWHM of O(1s), Si(2p), $Ti(2p_{3/2})$ and $Zn(2p_{3/2})$ are reported in Table 5. In order to compare the spectra a very small quantity of graphite powder was mixed with samples to furnish an internal standard (C 1s at 285 eV).

The high-resolution XPS spectra show an almost complete coincidence of C1 with C4 and of C2 with C5, as the calcination led to an extensive surface reconstruction, also where zinc is present inside the framework, whereas some slight differences are observed between C0 and C3. In particular, as reported in Table 5, the Si, O and Ti peak signals of C3 have a higher FWHM, pointing so out at the surface a greater chemical heterogeneity. The comparison among the C3–C5 spectra, relative to O, Si, Ti and Zn, is reported in Fig. 6. The peaks of C3 (green) are all systematically larger, those of C4 (blue) narrower, whereas those of C5 (pink) separated, showing up at least a second contribution at lower BE. It is so reasonable to assert that peak components are two and peak decomposition becomes essential to obtain clear spectroscopic data. Table 6 reports for Si(2p), O(1s), Ti(2p) and Zn(2p) the results of decomposition: a main contribution and a secondary one shifted at lower binding energy. For C5 sample, where the peak profiles clearly show the separation shoulder, this shift is evaluated to be −2.1 eV (Si), −2.1 eV (O), −2.7 eV (Ti) and −2.3 (Zn) eV. Therefore, it is possible to suppose that *satellite* components correspond to particular species which experience a different surface electrostatic potential, induced by negative charges [27]. Reconsidering the undecomposed Zn peaks, Table 5 shows that the $Zn(2p_{3/2})$ BE peak value of C3 is higher (+0.8 eV) when compared with ZnO standard (BE 1022.8 eV) one, but lower (−0.9 eV) than $Zn(OAc)_2{\cdot}2H_2O$ (BE 1024.5), thus suggesting the presence of both Zn–O bonds and positively charged species. In the case of C4 and C5, calcined at 823 and 1073 K, respectively, the Zn(2p) BE value is 1023.1 eV, very similar (+0.3 eV) to that of ZnO, from which it cannot be inferred the presence of a local positive charge on Zn-coordinated in TS-1 framework. Knowing by XRPD that ZnO phase has not been observed and α-willemite (Zn_2SiO_4) phase has formed at the higher temperature, we can reasonably suppose the existence of Zn–O–Ti and Zn–O–Si bonds. Literature data report for willemite Zn 2p peak at 1022.7 eV BE [28].

The Auger signal of Zn LMM was also evaluated for C3–C5 samples, for the Auger parameter calculation. Combining data of kinetic energy (986.8, 987.2, 988.1 eV, respectively) with Zn 2p

Table 5
XPS: binding energy and FWHM of O, Si, Ti and Zn

	Calcinated for 5 h (K)	O(1s)		Si(2p)		$Ti(2p_{3/2})$		$Zn(2p_{3/2})$	
		BE (eV)	FWHM (eV)	BE (eV)	FWHM (eV)	BE (eV)	FWHM (eV)	BE (eV)	FWHM (eV)
ZnO	No	531.7	1.0	–	–	–	–	1022.8	1.8
$Zn(OAc)_2{\cdot}2H_2O$	No	533.7 531.6	1.5 2.0	–	–	–	–	1024.5	2.6
C0	No	532.7	2.5	103.6	2.4	459.8	2.7	–	–
C1	823	532.8	2.5	103.6	2.3	459.8	3.0	–	–
C2	1073	532.8	2.3	103.6	2.3	459.9	2.5	–	–
C3	No	533.2	3.3	103.6	3.3	459.8	3.5	1023.6	3.7
C4	823	532.7	2.9	103.6	2.9	459.4	3.3	1023.1	3.0
C5	1073	532.8	3.0	103.6	3.0	460.0	3.0	1023.1	3.4

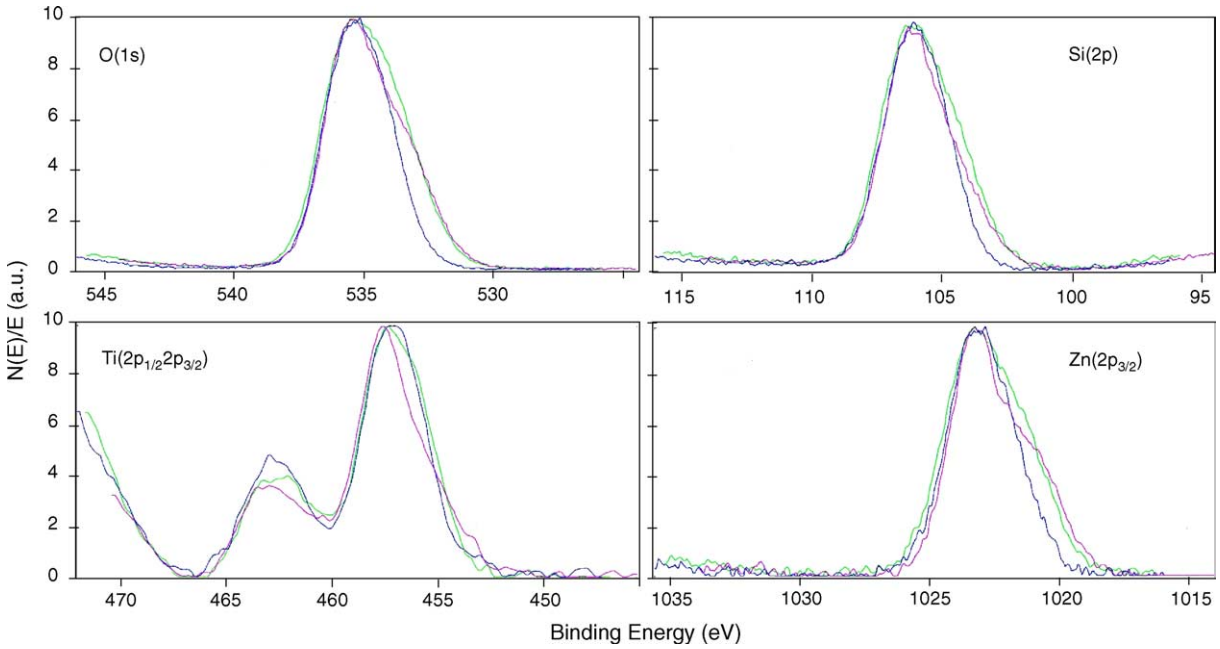

Fig. 6. High-resolution XPS spectra of C3 (green), C4 (blue) and C5 (pink) samples: O(1s), Si(2p), Ti($2p_{1/2}$ $2p_{3/2}$) and Zn($2p_{3/2}$). (For interpretation of the references to colour in this figure legend, the reader is referred to the web version of the article.)

Table 6
XPS: O(1s), Si(2p), Ti($2p_{3/2}$) and Zn($2p_{3/2}$) peak decomposition of C3, C4 and C5 samples

Sample no., calcination	O(1s)		Si(2p)		Ti($2p_{3/2}$)			Zn($2p_{3/2}$)		
	BE (eV)	FWHM (eV)	BE (eV)	FWHM (eV)	BE (eV)	FWHM (eV)	AREA (%)	BE (eV)	FWHM (eV)	AREA (%)
C3										
No	533.0	2.6	103.6	2.5	459.9	2.9	73	1023.4	2.7	64
Satellite	531.2	2.9	101.6	2.4	457.9	2.5	27	1021.3	2.7	36
C4										
823 K	533.2	2.4	103.6	2.6	459.8	2.9	80	1023.4	2.3	73
Satellite	531.7	2.3	102.1	2.0	457.9	2.7	20	1021.6	2.1	27
C5										
1073 K	533.0	2.3	103.6	2.5	459.9	2.9	79	1023.2	2.3	61
Satellite	530.9	2.7	101.5	2.6	457.2	2.7	21	1020.9	2.7	39

binding energy data (of Table 5) on a Wagner plot [7,29], Auger parameters with increasing values have been found (2010.2 for C3; 2010.5 for C4; and 2011.2 for C5). This would suggest a stronger covalent character of C5 Zn–O bonds than for C4 and C3, which present a more ionic Zn–O bonds. A similar information is obtained analyzing the satellite components of the main peaks (Table 6).

As far as the Ti-signal is concerned in all samples only the main contribution due to Ti(IV) in tetrahedral configuration (459.9 ± 0.1 eV) has been observed [30,31]. Neither at 823 K nor at 1073 K the presence at the surface of Ti(IV) in hexahedral configuration (458.4 eV BE) was evident, even if Ti-concentration increases from 0.7 to 1.1 wt% in the case of Zn-treated samples.

3.5. Sorption simulation

The simulation of the adsorption in the crystal frames evidences that the $[Zn(OH)]^+$ and H_2O adsorbates are retained inside channels in large quantity, but with different ratio between S-1 and TS-1. In the case of the TS-1 there is an increase of $[Zn(OH)]^+$ molecules number per elementary cell, whereas the H_2O ones reduces (Table 7). The ratio $R([H_2O]/[Zn(OH)]^+)$ between concentrations of the two sorbates, is smaller for TS-1 and this implies a lower positive charge on the average, because a part of this is shared in the bond between titanium atom and zinc complex, with the result of a smaller number of H_2O solvation molecules. $[Zn(OH)]^+$ species exhibits the tendency to coordi-

Table 7
Sorption simulation: $[Zn(OH)]^+$ and H_2O adsorbates in S-1 and TS-1

	H_2O (molecules/ elementary cell)	$[Zn(OH)]^+$ (molecules/ elementary cell)	$R([H_2O]/[Zn(OH)]^+)$
S-1	12	10.5	1.14
TS-1	10	13.0	0.77

nate with second molecule of the same type, as in the scheme below:

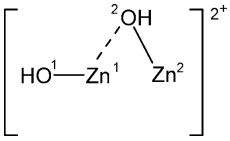

The coordination distance between two $[Zn(OH)]^+$ cations is about 3 Å, with the lowest values of 2.6 Å for $Zn^1\cdots Zn^2$ and 2.4 Å for $Zn^1\cdots O^2$, where the one between $[Zn(OH)]^+$ and H_2O ($Zn\cdots OH_2$) is 2.3 Å.

The analysis of the average picture coming out from the calculations shows that these species are distributed inside the framework and, in particular, in the 10-ring channels where diffusive processes take place. However, $[Zn(OH)]^+$ or $[Zn(OH)]^+\cdots OH_2$ cations are present also inside the pentagonal rings, pointing out that these are coordination sites even if they are often considered inaccessible. $Zn\cdots Ti$ distance displays minimum value of 2.8 Å, respect to 3.0 Å for $Zn\cdots Si$ one. Introduction in the cell of two titanium atoms, in the T8 and T11 sites, instead of one, does not change the system description both as aggregation and spatial distributions.

3.6. Quantum mechanical calculations

A neutral model was chosen to describe the electronic properties: in this H_2O and $Zn(OH)_2$ interact with the two complexes which represent S-1 and TS-1, respectively. The choice of neutral $Zn(OH)_2$, rather than charged $Zn(OH)^+$ species, derives on one hand from the fact that the calculation involving the cation and one H_2O molecule has given an energetically very unstable system, on the other hand the $Zn(OH)^+$ species is most probably stabilized by solvation shell. The energy minimization of the two solvates interacting with Si(IV) or with tetrahedral Ti(IV), isomorphous to it, has given an interaction energy between $Zn(OH)_2$ of −5.3 kcal/mol in the case of S-1 complex, and of −4.3 kcal/mol in the case of the TS-1 complex. It is observed the interaction energy is not higher than that of hydrogen bond between two H_2O molecules, that is about −5 kcal/mol. Although the energy is very similar, the analysis of molecular orbitals population shows a significant difference. Fig. 7 displays the valence molecular orbitals which are formed by the interaction between the $Zn(OH)_2$ and H_2O ligands and the complex, S-1 (a) or TS-1 (b). These correspond to orbitals that are very close in energy to the Fermi level. It is evident the absence of charge density in the $[Zn(OH)_2]\cdots Si(IV)$ bond orbital, in fact, as showed in (a), the silicon atom is visible being not hidden by electronic density cloud. On the contrary, in the case of TS-1 (b), the Ti 3d orbitals take part with the Zn ones in formation of oxygen coordination bond. In other words, the Ti atom is partially covered and the interaction between the two metals is mediated by the oxygen of $Zn(OH)_2$, involving the Ti 3d orbitals as visible from orbital extent from Ti to O in Zn(OH) (b). Moreover, compared with the silicon, the distribution of distances between $Zn(OH)_2$ ligands and Ti-site is always shifted towards shorter ones, coherently with the higher grade of orbital superposition, as well as a narrower O–Zn–O angle (in TS-1 128.8° and in S-1 146.2°).

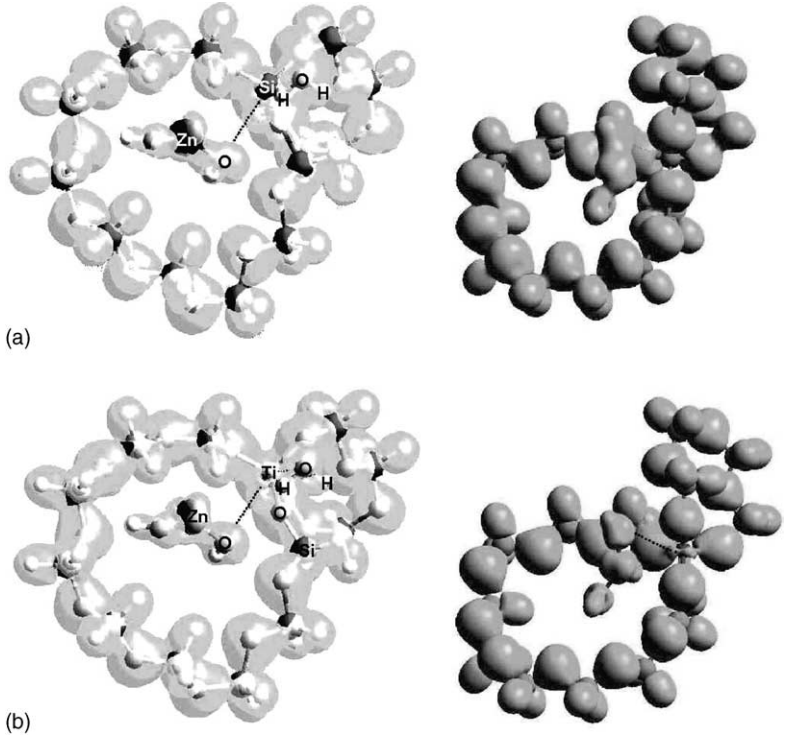

Fig. 7. (a) S-1 and (b) TS-1: valence molecular orbitals of outer states in the range from −5.0 eV to Fermi level; the grey isosurface showing the orbitals is contoured at 0.1 electron.

3.7. Zn-aqueous solution chemistry and ion exchange between $[Zn(OH)]^+$ and silanol or titanol proton assisted by acetate base

Zinc cation does not experience any ligand field stabilization effect ($3d^{10}$ filled orbitals) and its stereochemistry is essentially determined by electrostatic forces with the ligands (Brönsted bases). Zn^{2+} solvation energy in water is enough to allow the coordination expansion to 5 (*Trigonal-Bipyramidal* symmetry) or up to 6 (*Octahedral* symmetry). The field strength weakens hydrogen–oxygen bond in water molecules, bringing to hydrolysis and increasing Brönsted acidity

$$[Zn(H_2O)_4]^{2+} + H_2O \rightleftarrows [Zn(H_2O)_3(OH)]^+ + H_3O^+ \quad (1)$$

In S-1 and TS-1 crystal ion exchange may occur between $[Zn(OH)]^+$ or $[Zn(H_2O)_3(OH)]^+$ and silanol or titanol proton assisted by acetate base, as reported in (2):

$$\equiv Si(Ti) - O^{\delta-} \cdots {}^{\delta+}H + Zn(OH)^+ \overset{CH_3COO^-}{\rightleftarrows} \equiv Si(Ti)\text{–}OZn(OH) + CH_3COOH \quad (2)$$

The next calcination at 823 K causes condensation reactions with water and acetic acid removal from catalyst (3), as shown by TGA analysis, leaving the zinc atom bonded to vicinal oxygens of the crystal frame.

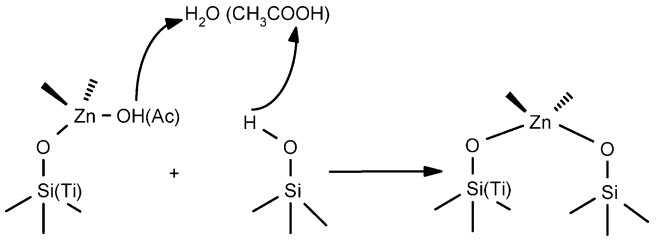

(3)

This process leads to an increase of catalyst aqueous slurry apparent pH from 4.5 to 6.7 (Table 1).

3.8. Interaction between Zn hydrate complex ion and framework

$Zn^{2+}/[Zn(OH)]^+$ cations in S-1 and TS-1 can coordinate to the structure introducing a local positive charge density (δ^+). Quantomechanical calculation points to the $[Zn(OH)]^+$ coordination on isomorphous Ti(IV) in TS-1 occurs via interaction between Ti 3d and Zn 3d orbitals mediated by oxygen of Zn–O–H. Moreover by adsorption simulations the ratio $R([H_2O]/[Zn(OH)]^+)$, with concentrations expressed as molecules/elementary cell, is 0.77 in TS-1 and 1.14 in S-1, indicating a smaller fractional charge is involved in the bond between titanium and zinc complex so a lower salvation is necessary. The theoretical calculation shows the presence of $[Zn(OH)]^+$ cation or of its hydrate form $[Zn(OH)]^+ \cdots OH_2$, inside 10-ring channels where the diffusion mainly occurs, and also in 5-ring structure, generally assumed to be not accessible. The proposed reaction (4) shows the interaction between Zn complex cation and Ti-site

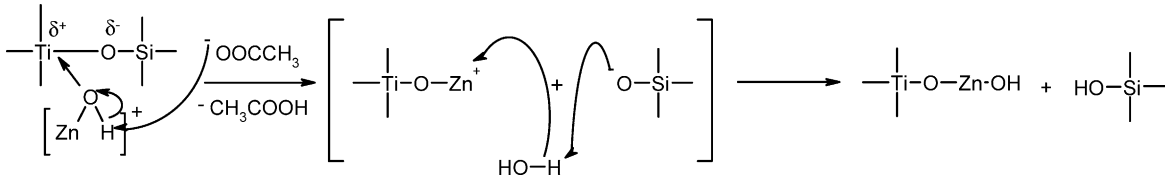

(4)

In agreement with reaction (4), the $Zn(2p_{3/2})$ BE peak value at 1023.6 eV (C3, Table 6) and the 2010.2 value of Auger parameter suggest the presence of Zn–O bonds having some positive ionic character. So, the subsequent calcination at 823 K would determine the insertion of zinc atom between two oxygens,

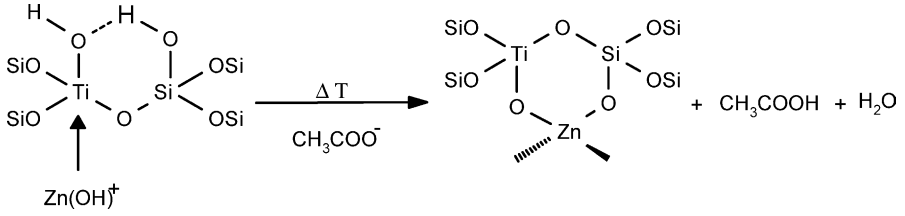

(5)

as already shown in (3). XRPD and DRS/UV–vis analyses do not evidence the presence of ZnO phase, whereas XPS confirms Zn–O bond presence related to Zn–O–Ti(Si) bonds with lesser ionic character respect to the uncalcined TS-1. Moreover, the DRS/UV–vis absorption profile does not change significantly, pointing to that titanium is still in tetrahedral configuration (210 nm, LMCT transition), in agreement with XPS results. At 823 K, Zn–O–Ti bonds could form to give $ZnTiO_3$ ordered structures, fully crystallized at 1073 K [32]. In our sample, $ZnTiO_3$ crystalline phase was not observed also after the thermal treatment at 1073 K: on the contrary, α-willemite crystalline phase (Zn_2SiO_4, zinc orthosilicate) was detected by XRPD. Titanium in TS-1 seems to promote specifically the α-willemite formation, lowering its activation energy, not observed in S-1 [19]. At 1073 K, ZnO crystalline phase is not evident (XRD and DRS/UV–vis) and Zn–O bonds from XPS analysis can be assigned to the α-willemite phase. Rietveld refinement of XRPD

Table 8
Epoxidation: rapid reaction test

	TS-1 zinc salts treatment			
	No	Zinc carbonate $2ZnCO_3{\cdot}3Zn(OH)_2$ (suspension)	Zinc acetate $Zn(OAc)_2{\cdot}2H_2O$ (incipient wetting impregnation)	Zinc nitrate $Zn(NO_3)_2$ (percolation)
Zn(II) in TS-1 via XRF (wt%)	–	0.07	0.07	0.06
Catalyst aqueous slurry (apparent pH)	4.5	6.7	6.7	6.6
H_2O_2 conversion (mol%)	96.0	97.0	96.6	97.2
Selectivity to 1,2-epoxypropane (mol%)	93.0	98.2	98.5	98.1
Yield of by-products (ethers + glycols) (mol%)	6.5	1.5	1.2	1.6

spectra have shown that Zn-treated TS-1 keeps an open structure with 5370 $Å^3$ cell volume also after thermal annealing at 1073 K, contrary to all occurs for H_2O-treated TS-1.

3.9. Epoxidation of propylene

Our experimental results show that epoxidation reaction proceeds with an increased selectivity in the presence of Zn-treated TS-1, remaining substantially unaltered the H_2O_2 conversion (96–97 mol% range, from rapid epoxidation test, Table 8). Selectivity to 1,2-epoxypropane (PO) increases from 93 to 98.5%, apart from preparation procedure and zinc salt used, with a parallel decrease of by-products concentration (from 6.5 to 1.5 mol%, Table 8 and Fig. 9).

Ab initio quantum mechanical calculations on Zn/TS-1 cluster model, including Ti–OOH [33,34], were carried out to get more insight on the catalysis mechanism. Fig. 8 shows the model where zinc and methanol are coordinated to the titanium atom situated in T11 site. A five-membered cyclic complex (**I**) between Ti–OOH and methanol has been considered, Scheme 1, in analogy both with Clerici-like ring in heterogeneous phase [35,36] and with very similar ring proposal in homogeneous phase by metal-peroxo species (MOOR) formation (M = Ti, Zr, V, Mo, W or Pd and Pt) [37].

The analysis reveals an interaction energy of −46 kcal/mol between CH_3–OH and Ti–OOH site that becomes −64 kcal/mol when zinc is present. The distances between titanium and ligand in Ti–O–Zn or Ti–O–Si models are reported in Table 9. The Ti···O3 distance between methanol and titanium does not change, resulting 2.08 Å in TS-1 and 2.11 Å in Zn/TS-1, as well as the Ti···O5Si distances (2.17 and 2.20 Å, respectively). These last distances indicate the silanol leaving group has to be considered more properly as sixth ligand to Ti atom [38]. In particular, referring to Clerici-like ring (**I**, Scheme 1), it is observed that the O2···H3 distance between hydroperoxide (O2) and methanol (H3) in TS-1 and Zn-treated TS-1 is too long, about 3.6 Å, to justify the formation of a cyclic complex as Clerici's one. These evidences would lead towards a cycle in which the silanol rather than the alcoholic group of methanol closes on the peroxide ligand, apart from zinc presence (**II**, Scheme 1). In fact, the distance between O2 peroxide group and hydrogen of silanol (O2···H5–O5Si) is much shorter (about 2.8 Å) than O2···H3 (3.6 Å).

It is worthy of notice the distance H3···O5Si between alcoholic hydrogen (H3) and silanolic oxygen (O5), are 2.67 and

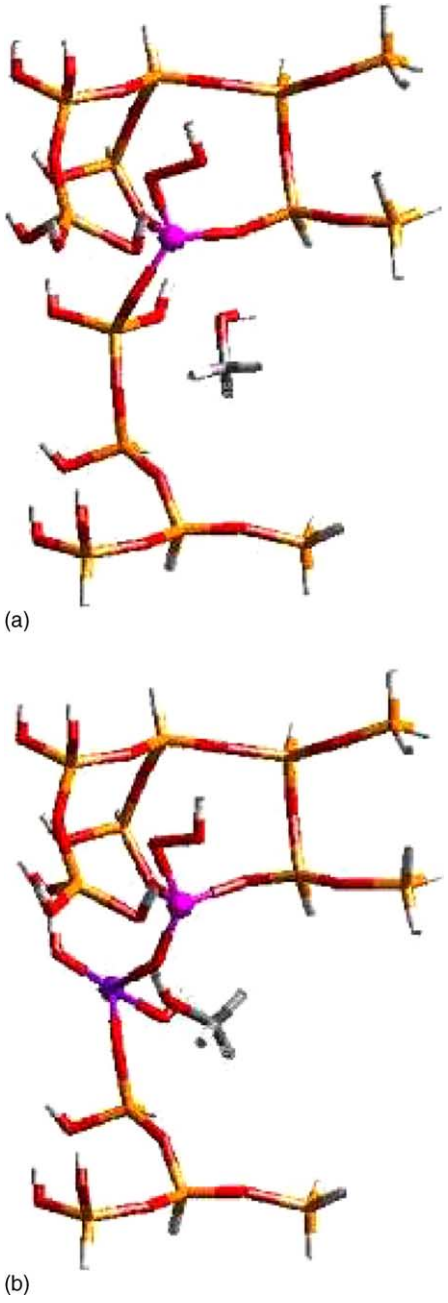

Fig. 8. (a) methanol coordination to Ti–OOH site (Ti in magenta) in TS-1 and (b) methanol coordination to Ti-OOH site with zinc (purple) is in the framework (Zn/TS-1). (For interpretation of the references to colour in this figure legend, the reader is referred to the web version of the article.)

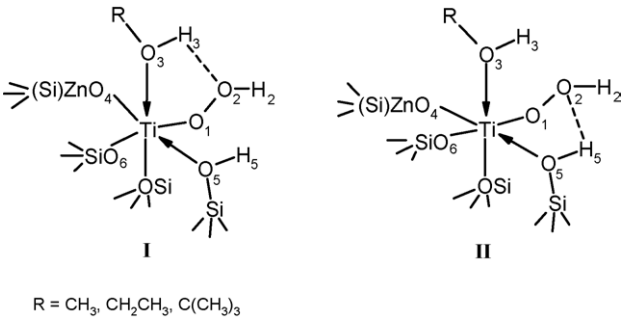

Scheme 1.

Table 9
Ab initio quantum mechanical calculation: distances at Ti–OOH site in TS-1 and Zn/TS-1 models, as indicated in Schemes 1 and 2

	Distances (Å)	
	TS-1	Zn/TS-1
Methanol···Ti–OOH		
Ti–O1	1.74	1.72
O1–O2	1.45	1.51
O2···H3	3.50	3.60
H3–O3	1.06	0.98
O3···Ti	2.11	2.08
Silanol···Ti–OOH		
Ti–O1	1.74	1.72
O1–O2	1.45	1.51
O2···H5	2.80	2.79
H5–O5	0.89	0.86
O5···Ti	2.17	2.20
O3–R	1.40	1.44
H3···O4	3.05	3.50
H3···O5	2.67	3.17
H5···O4	3.38	3.20
H5···O3	2.67	2.76
O4···O3	2.41	2.55
O3···O5	2.59	2.65
O4···O5	2.68	2.44

3.17 Å in TS-1 and Zn/TS-1, respectively, to indicate a hydrogen interaction between the respective hydroxyls. It is observed that these distances are very similar to the O2···H5O5Si ones (2.8 Å) suggesting that silanol is shared between methanol and Ti–OOH group, as indicated in Scheme 2, forming at Ti-active site a more extended cycle.

Moreover, the H3···O5Si higher distance found in Zn/TS-1 justifies a more relaxed situation, in agreement with a more open structure, as it results from the higher cell volume (5370 Å) calculated for Zn-treated TS-1.

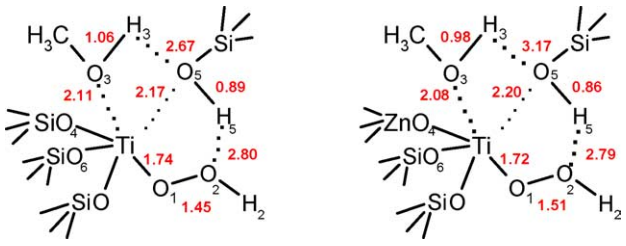

Scheme 2.

The calculated values of energy for CH_3–OH···Ti–OOH (−46 and −64 kcal/mol when zinc is present) result relatively high, because they refer to the interaction between the solvent molecule and model-cage from which the energy of the two isolated components has been subtracted, without allowing each one's geometry relaxation, and not taking into account basis set superposition error. As a consequence, the relative energetic differences between the alcohol TS-1 complex and alcohol Zn/TS-1 ones have to be considered, more than the numerical values. The increased interaction energy of methanol at Ti-site when zinc is present implies a Ti–OOH electrophilicity reduction, in agreement with our experimental kinetic results. In fact, as shown in Fig. 9, the data indicate clearly a selectivity fully in favour of PO when TS-1 is Zn-treated, even if a double time is necessary to convert a same H_2O_2 concentration. All that is also well evidenced from the relative by-product formation. The already observed epoxidation order that decreased in the sense MeOH > EtOH > *n*-PrOH > *i*-PrOH > *t*-BuOH as resulted of decreasing Ti–OOH electrophilicity [35,36] can be explainable by our model, but this effect becomes more important when

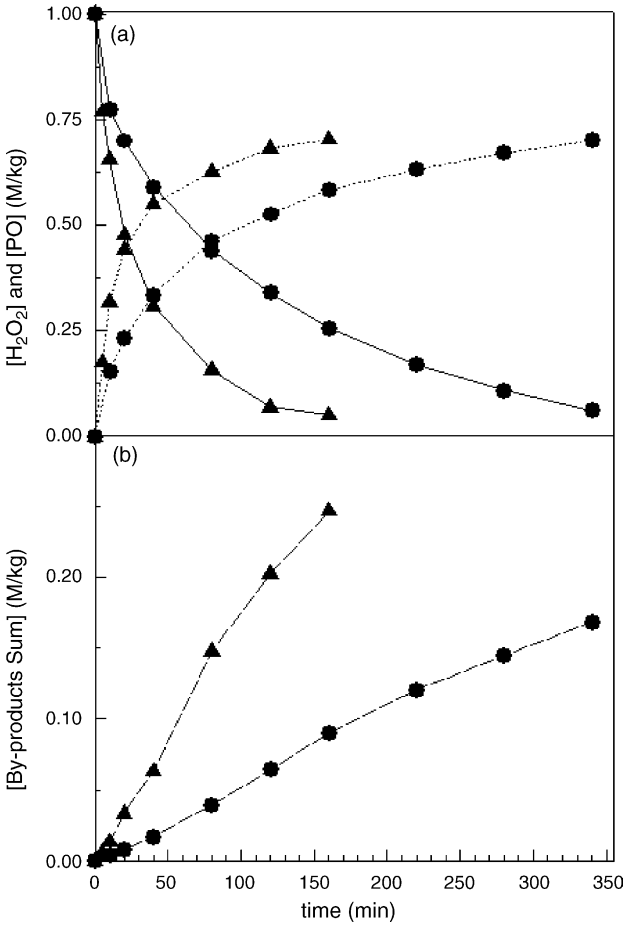

Fig. 9. Epoxidation of propylene with H_2O_2 in methanol/water at 40 °C: reaction with TS-1 (▲) and Zn/TS-1 (●) catalysts; (a) PO yield (full line) and H_2O_2 conversion (dotted line); (b) by-products in epoxidation (sum of propylene glycol, 1-methoxy-2-propanol and 2-methoxy-1-propanol).

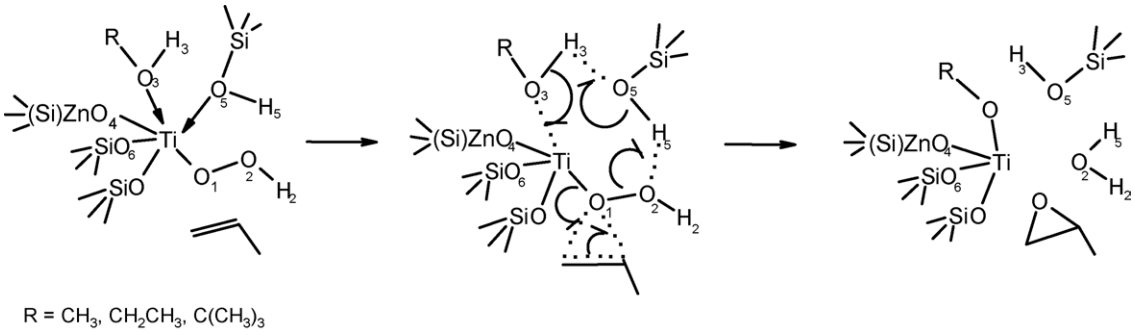

Scheme 3.

the zinc is presence. At the same time the acidity of TiOO–H group and its exchange ability with alkali metal salts should remain qualitatively unchanged.

On the strength of all these evidences the epoxidation reaction can occur through a transition state at Ti-site in which hydroperoxide, alcoholic group, silanol and propylene are involved, as shown in the following reaction Scheme 3.

We propose the pathway can occur by a step in which hydroperoxide intermediate reacts with propylene by proximal O1 oxygen abstraction, greatly facilitated by a concerted electronic rearrangement and protonic transfer involving silanol and alcoholic groups to give water, as depicted in Scheme 3. This transition state involves six-fold oxygen coordination on Ti-site from which we retain the less constrained Ti environment, relaxed to a major octahedral geometry, can justify a higher stability of the transition state. The electrophilic attack on the propylene double bond is the assumed mechanism for oxygen abstraction. Our epoxidation route suggests that the proximal O1 oxygen is involved in the interaction with C=C bond, because in this bond situation O1 is more electron deficient with respect to the distal O2. In fact, O1 suffers of the O2 increased electron withdrawing effect resulting from its interaction with H5, strongly electron-poored by the O5 coordination on Ti. Recently, DFT study on propylene epoxidation on a defective Ti-site in TS-1 due to a silicon vacancy has proposed a similar transition state but suggesting a simultaneous dual hydride transfer mechanism to justify the oxygen abstraction by propylene [39]. The enhanced donor property of solvent on Ti-site when zinc is present seems supporting our electronic rearrangement more than a hydride path. After rearrangement, Ti-site brings the alkoxide group (Ti–O–R) that immediately by H_2O_2 entrance restores the Ti–OOH site and coordinated methyl alcohol.

3.10. By-products formation

As reported in Table 8 and Fig. 9, a drastic reduction of by-products, when the TS-1 is Zn-treated, is observed. For a better understanding of by-product reduction during the reaction, PO stability test was performed contacting PO and H_2O_2 in the presence of Zn-treated and untreated TS-1 and the results are summarized in Table 10. The Zn-effect was observed on PO recovery after 6 h of permanence time at 313 K. The contact among Zn/TS-1/PO/H_2O_2 reduces the initial PO concentration at 72 mol%, and at 55 mol% for the one among TS-1/PO/H_2O_2. By-products, including the higher oligomers, are then 28 and 45 mol%, respectively. Also, turn over frequency (TOF) on Ti-site was valuated from kinetic test using TS-1 and Zn/TS-1 pre-treated with 4.5 wt% PO (Table 11). At 90% conversion of the initial H_2O_2, the PO treatment reduces TOF by 25% in the case of TS-1 and by 6.5% in the Zn/TS-1 one. So, on untreated TS-1 a four-fold amount of oxiranic ring opens promoting the glycol formation. These evidences could be explained assuming a fraction of propylene oxide just formed remains partially coordinated on the Ti-site by oxiranic oxygen interaction. On regard, our calorimetric experiments performed in methanol/water solution contacting TS-1 and propylene oxide (PO) give a heat release of about 7.2 kcal/mol, justifying this interaction at Ti-site. This result is in agreement with the value of 5.5 kcal/mol for ethylene oxide (EO) found by Neurok and Manzer [40] via DFT calculation when EO is formed. The difference between two values can be due to the higher PO Lewis basicity than EO. The interaction between the just PO formed and TS-1 can be then considered the initial step of degradative reaction path, by epoxide ring opening, giving the 1-methoxy-2-propanol, 2-methoxy-1-propanol, 1,2-propanediol and higher oligomers by-

Table 10
PO stability test[a] in MeOH/H_2O solution contacting TS-1 and Zn-treated TS-1

	TS-1	Zn-treated TS-1
MeOH/H_2O solution[b] + PO + catalyst [(90 + 5 + 5) wt%]		
Loaded catalyst (g/kg)	3.73	3.70
Products (mol%)		
Residue PO	83.26	94.28
1M-2P	2.42	1.83
2M-1P	10.00	3.42
PG	1.53	0.47
Balance	97.21[c]	100.00
MeOH/H_2O solution[b] + H_2O_2 + PO + catalyst [(85 + 5 + 5 + 5) wt%]		
Loaded catalyst (g/kg)	3.64	3.67
Products (mol%)		
Residue H_2O_2	98.30	98.77
Residue PO	54.62	72.27
1M-2P	13.09	8.07
2M-1P	15.70	9.53
PG	4.96	4.29
Balance	88.37[c]	94.16[c]

[a] Six-hour tests were performed in a hermetic sealed vessel, thermostated in a bath at 313 K and 170 times/min shaken.
[b] Solution: MeOH/H_2O (97/3, v/v).
[c] The imbalance to 100 is due to higher oligomers, herein not reported.

Table 11
Turn over frequency test on TS-1 and PO-pre-treated TS-1 respect to Zn/TS-1 and PO-pre-treated Zn/TS-1

Sample	PO selectivity at the H_2O_2 conversion of			Time (min)	Loaded catalyst (g)	TiO_2 (wt%)	PO producted (g)	TOF[a] (at 90% H_2O_2 conversion)
	50%	70%	90%					
TS-1	93.7	88.0	78.0	105	2.01	3.65	19.70	211
TS-1 4.5 wt% PO treated	92.5	85.2	72.5	120	2.01	3.65	16.38	158
Zn/TS-1	94.0	89.8	84.2	205	2.17	3.38	19.76	109
Zn/TS-1 4.5 wt% PO treated	92.8	87.2	81.8	220	2.17	3.38	19.88	102

[a] TOF calculated as (moles of PO producted/g_{atom} of Ti_{total} × time (h)), where Ti_{total} is framework-plus extraframework-Ti in catalyst.

products when the oxidation reaction proceeds, and justifying a reduced timing activity caused by Ti-active sites subtraction to the H_2O_2 reaction to give Ti–OOH. All of that results strongly reduced when zinc is present.

4. Conclusions

Direct propylene epoxidation with H_2O_2 performed on TS-1 pre-treated with zinc salts has disclosed a metal specific role. Experimental data (XRPD, DRS UV–vis, XPS) and quantum mechanical calculations have concordantly pointed out the zinc coordinates to Ti-site via oxygen, Zn–O–Ti(Si). This coordination takes place, i.e. in the case of zinc acetate salt, through two mechanisms that involve (i) an ion exchange between $[Zn(OH)]^+$ and silanol or titanol proton, assisted by acetate base and/or (ii) an interaction between Zn hydrate complex ion and Ti-site by $[Zn(OH)]^+$ oxygen, to which the thermal treatment follows.

The quantum mechanical calculations, performed on TS-1 structure in which zinc forms a Zn–O–Ti bond, reveals that the interaction energy between methanol and Ti–OOH site increases when zinc is present, with the consequence that the solvent increases its donor properties at Ti-site producing a reduced Ti–OOH electrophilicity. Leaving aside the zinc presence, the distance between the alcoholic hydrogen and the oxygen of hydroperoxide group is indeed too large to justify a well-defined Clerici-like ring. The silanol leaving group, which forms after H_2O_2 insertion, being so near the Ti-site, with and without zinc, behaves as sixth ligand to Ti atom. The geometry optimization leads to a more open cycle at Ti-site where silanol is shared between methanol and Ti–OOH group. We retain the propylene epoxidation can occur at Ti-site by a cyclic reaction scheme in which a hydroperoxide oxygen abstraction by propylene double bond is promoted by a concerted electronic rearrangement and protonic transfer involving silanol and alcoholic groups to form water. In this mechanism, the silanol plays a role in directing the double bond nucleophile attack preferably towards O_1 ($Ti–O_1O_2H$). The experimental kinetic results, clearly indicate a selectivity in favour of propylene oxide when Zn is present, even if a double time is necessary to convert the same H_2O_2 concentration, in agreement with Ti–OOH electrophilic reduction foreseen by our model. The lower by-product formation also confirms this.

Acknowledgements

The authors thank Dr. M. Ricci for the useful discussions and Polimeri Europa that allowed the publication of this work.

References

[1] F. Maspero, U. Romano, J. Catal. 146 (1994) 476.
[2] V. Hulea, P. Moreau, F. Di Rienzo, J. Mol. Catal. A 111 (1996) 325.
[3] W. Adam, A. Corma, T.I. Reddy, M. Renz, J. Org. Chem. 62 (1997) 3631.
[4] M.G. Clerici, P. Ingallina, Catal. Today 41 (1998) 351.
[5] M.G. Clerici, La Chimica e l'Industria 85 (2003) 55.
[6] M. Taramasso, G. Perego, B. Notari, U.S. Patent 4,410,501 (1983).
[7] J.F. Moulder, W.F. Stickle, P.E. Sobol, K.D. Bomben (Eds.), Handbook of XPS, Perkin-Elmer Corp., MN, USA, 1992.
[8] Perkin-Elmer Publication B2116, Release 4.0/June 1992.
[9] A.C. Larson, R.B. Von Dreele, GSAS—General Structure Analysis System, Los Alamos National Laboratories, No. LA-UR-86-748, NM (USA), 1998.
[10] R.A. Young (Ed.), The Rietveld Method, IUCr Monographs on Crystallography-5, International Union of Crystallography, Oxford Science Pubblication, 1996.
[11] Cerius 2 4.2, Accelrys Inc., San Diego (CA), 2001.
[12] M.C. Payne, M.P. Teter, D.C. Allen, T.A. Araias, J.D. Joannopolous, Rev. Mod. Phys. 64 (1992) 1045.
[13] C. Lamberti, S. Bordiga, A. Zecchina, G. Artioli, G. Marra, J. Spanò, J. Am. Chem. Soc. 123 (2001) 2204.
[14] J. Harris, Phys. Rev. B 31 (1985) 1770.
[15] A. Zecchina, S. Bordiga, G. Spoto, L. Marchese, G. Petrini, G. Leofanti, M. Padovan, J. Phys. Chem. 96 (1992) 4985;
A. Zecchina, S. Bordiga, G. Spoto, L. Marchese, G. Petrini, G. Leofanti, M. Padovan, J. Phys. Chem. 96 (1992) 4991.
[16] M.A. Simonov, P.A. Sandomirski, Yr.K. Egorov-Tismenko, N.V. Belov, Dolk. Akad. Nauk SSSR 237, 1977, p. 581, "α-willemite", Card No. 5106, WWW-MINCRYST, Crystallographic Database for Minerals, at web site http://database.iem.ac.ru/mincryst/index.php.
[17] D.J. Robbins, E.E. Mendez, E.A. Giess, I.F. Change, J. Electrochem. Soc. 131 (1984) 141.
[18] TiO_2 Rutile, Card No. 4028, WWW-MINCRYST, Crystallographic Database for Minerals, at web site http://database.iem.ac.ru/mincryst/index.php.
[19] C.C. Lee, P. Shen, H.Y. Lu, J. Mater. Sci. 24 (1989) 3300.
[20] L.R. Pinckney, U.S. Patent 6,303,527 (2001).
[21] C.K. Jφrgensen, Prog. Inorg. Chem. 12 (1970) 101.
[22] G. Leofanti, F. Genoni, M. Padovan, G. Petrini, G. Trezza, A. Zecchina, Stud. Surf. Sci. Catal. 62 (1991) 553.
[23] L.E. Brus, J. Chem. Phys. 80 (1984) 4403;
L.E. Brus, J. Chem. Phys. 90 (1986) 2555.
[24] E. Brendan, D. Fitzmaurice, J. Phys. Chem. 100 (1996) 1027.
[25] C. Kormann, D.W. Bahnemann, M.R. Hoffmann, J. Phys. Chem. 92 (1988) 5196.
[26] X.S. Zhao, G.Q. Lu, G.J. Millar, J. Porous Mater. 3 (1996) 61.
[27] L. Meda, F. Garbassi, L. Pozzi, G. Ranghino, Vuoto 26 (1997) 42.
[28] L.S. Dake, D.R. Bear, J.M. Zachara, Surf. Interface Anal. 14 (1989) 71.
[29] C.D. Wagner, L.H. Gale, R.H. Raymond, Anal. Chem. 51 (1979) 466.
[30] D. Trong On, L. Bonneviot, A. Bittar, A. Sayari, S. Kaliaguine, J. Mol. Catal. 74 (1992) 233.
[31] L. Le Noc, D. Trong On, S. Solomykina, B. Echchahed, F. Beland, C. Cartier dit Moulin, L. Bonneviot, Stud. Surf. Sci. Catal. 101 (1996) 611.

[32] Y.-S. Chang, Y.-H. Chang, I.-G. Chen, G.-J. Chen, Y.-L. Chai, J. Cryst. Growth 243 (2002) 319.
[33] L. Bonoldi, C. Busetto, A. Congiu, G. Marra, G. Ranghino, M. Salvalaggio, G. Spanò, B. Giamello, Spectrochim. Acta Part A 58 (2002) 1143.
[34] F. Bonino, A. Damin, G. Ricchiardi, M. Ricci, G. Spanò, R. D'Aloisio, A. Zecchina, C. Lamberti, C. Prestipino, S. Bordiga, J. Phys. Chem. B 108 (2004) 3573.
[35] G. Bellussi, A. Carati, M.G. Clerici, G. Maddinelli, R. Millini, J. Catal. 133 (1992) 220.
[36] M.G. Clerici, P. Ingallina, J. Catal. 140 (1993) 71.
[37] G. Strukul, La Chimica & L'Industria 72 (1990) 421.
[38] G.N. Vayssilov, R.A. van Santen, J. Catal. 175 (1998) 170.
[39] D.H. Wells Jr., W.N. Delgass, K.T. Thomson, J. Am. Chem. Soc. 126 (2004) 2956.
[40] M. Neurok, L.F. Manzer, Chem. Commun. 10 (1996) 1133.